JGR Atmospheres

RESEARCH ARTICLE
10.1029/2025JD044564

Special Collection:
Biomass Burning Uncertainties: Emissions, Chemistry, and Physics

Savannah and Boreal Biomass Burning as a Source for Cloud Condensation Nuclei

S. Peltokorpi[1], S. M. Kommula[1], A. Buchholz[1], L. Hao[1], M. Ihalainen[2], K. Jaars[3], K. Köster[4], E. I. Rosewig[5], S. J. Siebert[6], M. Somero[2], L. Vettikkat[1], P. Yli-Pirilä[2], P. G. van Zyl[3], J. Passig[5,7], R. Zimmermann[2,5,7,8], O. Sippula[2,8], V. Vakkari[3,9], and A. Virtanen[1]

[1]Department of Technical Physics, University of Eastern Finland, Kuopio, Finland, [2]Department of Environmental and Biological Sciences, University of Eastern Finland, Kuopio, Finland, [3]Atmospheric Chemistry Research Group, Chemical Resource Beneficiation, North-West University, Potchefstroom, South Africa, [4]Department of Environmental and Biological Sciences, University of Eastern Finland, Joensuu, Finland, [5]Joint Mass Spectrometry Centre, Chair of Analytical Chemistry and Department Life, Light & Matter, University of Rostock, Rostock, Germany, [6]Unit of Environmental Sciences and Management, North-West University, Potchefstroom, South Africa, [7]Joint Mass Spectrometry Centre, Helmholtz Centre Munich, Comprehensive Molecular Analytics, Oberschleissheim, Germany, [8]Department of Chemistry and Sustainable Technology, University of Eastern Finland, Joensuu, Finland, [9]Finnish Meteorological Institute, Helsinki, Finland

Key Points:

- Laboratory measurements on biomass burning particles show that the hygroscopicity parameter κ is higher with higher combustion efficiency
- The effect of aging on κ depends on the chemical composition of the fresh particles and is observed to decrease the overall variability in κ
- Cloud condensation nuclei emission factors show a decreasing trend with increasing combustion efficiency within savannah fuels

Supporting Information:

Supporting Information may be found in the online version of this article.

Correspondence to:

S. Peltokorpi and A. Virtanen,
saara.peltokorpi@uef.fi;
annele.virtanen@uef.fi

Citation:

Peltokorpi, S., Kommula, S. M., Buchholz, A., Hao, L., Ihalainen, M., Jaars, K., et al. (2026). Savannah and boreal biomass burning as a source for cloud condensation nuclei. *Journal of Geophysical Research: Atmospheres*, *131*, e2025JD044564. https://doi.org/10.1029/2025JD044564

Received 10 JUN 2025
Accepted 10 FEB 2026

Abstract Aerosol particles emitted in wildfires can contribute to radiative forcing via aerosol-cloud interactions and by directly interacting with solar radiation. Wildfire emissions increase the concentration of cloud condensation nuclei (CCN) in the atmosphere and thus affect cloud properties (e.g., cloud brightness). For this study, we conducted open laboratory burning experiments with less studied biomass types from South African savannah and European boreal forest, to quantify the particle hygroscopicity, an important factor affecting CCN concentrations. We also investigated the effect of burning conditions (characterized by the modified combustion efficiency (MCE)) and aging on the hygroscopicity of the particles. Considering all the experiments, the primary hygroscopicity parameter κ is constant (0.079 ± 0.007 (mean $\pm$ STD) for supersaturation of 0.43%) with respect to MCE for particles from smoldering combustion and increases to a maximum of 0.19 with increasing contribution of flaming. With aging, the hygroscopicity increases (boreal forest biomass) or remains unchanged (savannah biomass) in smoldering experiments, while it decreases in experiments with more flaming-dominated burning, decreasing the overall variability in κ. Using complementary chemical analysis methods, we provide insights into the markedly different CCN results under different burning conditions. Our results indicate that even in organic carbon-dominated aerosol representative of wildfires, a small fraction of inorganic material can significantly influence the aerosol hygroscopicity, highlighting the impact of combustion efficiency on biomass burning aerosol CCN activity.

Plain Language Summary Wildfires emit particles that can act as cloud condensation nuclei (CCN) and therefore increase the cloud fraction and lifetime, resulting in a cooling effect on the climate. The ability of a particle to act as CCN depends, for example, on its size and chemical composition. We investigate the effect of the chemical composition by studying the hygroscopicity of biomass burning particles. Samples of biomass from the South African savannah and the surface layer of a European boreal forest were burned in a laboratory and the emissions were analyzed using a chamber simulating the atmosphere. The hygroscopicity of the produced particles was low to moderate, consistent with their high organic fraction. The particles emitted from flaming-dominated burning were more hygroscopic compared with those from smoldering-dominated burning. As these particles age in the atmosphere, the resulting effect on hygroscopicity depends on the burning condition. The hygroscopicity of the particles from flaming-dominated burning decreases, while that of the particles from smoldering-dominated burning increases or stays the same. Our results highlight the impact of combustion efficiency on biomass burning aerosol CCN activity.

1. Introduction

Biomass burning (BB), including wildfires and residential combustion, is a major source of primary organic aerosol and black carbon (BC) worldwide (Andreae, 2019). It also emits a variety of gaseous compounds. Some of these compounds are strong greenhouse gases and others can act as precursors for secondary organic aerosol

(SOA) formation. During recent decades, the rate and intensity of wildfires have been increasing and are expected to further increase due to climate warming (Descals et al., 2022; Tyukavina et al., 2022). This warming is especially fast in arctic regions (Rantanen et al., 2022), making boreal forest fires an object of special interest. On the other hand, open fires in the savannah and grasslands are estimated to account for more than a third of the total annual burned biomass (Andreae, 2019), highlighting the importance of these biomes.

Aerosol particles emitted by wildfires can directly influence the global radiative budget of the Earth by scattering and absorbing radiation (Bellouin et al., 2005; Penner et al., 1998). These particles can also change the cloud properties by acting as cloud condensation nuclei (CCN) (Engelhart et al., 2012; Kommula et al., 2024) and therefore have an indirect effect on the climate. CCN activity of aerosols is influenced by the particle size, chemical composition, and mixing state (Ching et al., 2017; Petters & Kreidenweis, 2007). These properties, and therefore the CCN activity, have been observed to vary greatly depending on the burned fuel (e.g., Engelhart et al., 2012) and the burning condition (e.g., Gomez et al., 2018; Mouton et al., 2023).

The effect of chemical composition on the particle CCN activity, characterized with the hygroscopicity parameter κ, has been investigated in numerous studies both in field studies in the vicinity of wildfires (Gomez et al., 2018; Hsiao et al., 2016; Lathem et al., 2013; Rose et al., 2010) and in laboratory experiments (Dusek et al., 2011; Engelhart et al., 2012; Giordano et al., 2013; Martin et al., 2013; Mouton et al., 2023; Petters et al., 2009). In these studies, various biomass types are investigated, but only some include characterization of the burning condition. Despite several studies on the CCN activity of BB aerosols, there is a lack of research using fuels typical for savannah and grassland fires as well as for European boreal forest surface layer fires, especially in smoldering conditions.

Atmospheric aging can further alter the composition, size and mixing state of the aerosol and thus change their CCN activity (e.g., Che et al., 2022; Hodshire et al., 2019; Vakkari et al., 2014, 2018; Wu et al., 2021). If it rises above the boundary layer, BB smoke can be transported far from the source (Damoah et al., 2004). Wildfires can thus have severe effects on the climate and human health not only in the source region but also globally. This effect has been observed in the Arctic region (Gramlich et al., 2024; Kommula et al., 2024), where long-range transported BB emissions are an important source of aerosol during summer (Warneke et al., 2009, 2010). Another instance is South America, where the smoke transported from northern Africa has been observed to elevate CCN concentrations (Royer et al., 2023). Transported BB aerosol can be hours to even several days old and have significant effects on the climate (Farley et al., 2022). Thus, the aging of the wildfire emissions is especially important to consider when characterizing the CCN activity of long-range transported smoke aerosol particles.

Very few studies have investigated the CCN emission factors (EF_{CCN}), a parameter relating the number of emitted CCN active particles to the amount of burned biomass, for different biomass types. Andreae (2019) reported EF_{CCN} (0.5% SS) values of 0.8×10^{15} kg^{-1} for savannah and grassland fires, and 1.6×10^{15} kg^{-1} for boreal forest fires. A linear relationship between emission factors for particles larger than 100 nm, which can be used as an estimate for EF_{CCN}, and combustion efficiency was shown by Janhäll et al. (2010). Highly variable EF_{CCN} values for biomass combustion in cookstoves were reported by Kristensen et al. (2021). More studies are needed to better understand and quantify the emission factors of CCN active particles for different biomass fuels as well as the burning conditions.

For this study, we conducted laboratory measurements of BB emissions using African savannah originated woody and grassy material as well as samples of a boreal forest surface layer to investigate the particle hygroscopicity and CCN emission factors. We relate these properties to the combustion efficiency as it has been previously shown to greatly influence the emission properties. Additionally, utilizing an atmospheric chamber, we studied the impact of photochemical and dark aging on the particle hygroscopicity. With the unique boreal forest sample type containing vegetation, litter, and humus, we aim to mimic the field conditions of North European boreal forest surface fires more precisely than before. Overall, our findings extend prior research by adding data for African savannah and European boreal forest fuels and by showing the effects of combustion conditions and aging of the BB smoke on the hygroscopicity of aerosol emissions.

2. Methods

2.1. Biomass Samples and Combustion

Laboratory measurements of BB smoke were carried out as part of the Boreal And Savannah Fire Aerosol Aging (BASFAA) measurement campaign at the ILMARI research facility in Kuopio, Finland in May–June 2022. During the measurements, three biomass types, typical for savannah and boreal forest surface fires, were used. The savannah biomass was collected in South Africa close to the Welgegund measurement station (e.g., Jaars et al., 2016) and divided into grass and wood samples. The grass samples were collected from the ground and middle layer and the wood samples from the middle layer and the canopy. The boreal forest surface samples were collected in Evo, Finland from an experimental burn area (Köster et al., 2024) and consisted of forest surface vegetation, litter, and soil organic horizon. Prior to measurements, all the boreal samples were dried in an oven at 60°C. One sample of each biomass was chosen for the analysis of the total moisture. The savannah wood sample had a total moisture of 9.4% and savannah grass 8.6%, while the total moisture of the boreal forest surface sample was 9.6%.

For the combustion, the sample was placed on steel mesh under a hood with an open chimney leading to an atmospheric chamber. The sample was ignited using a heated resistor. By controlling the ignition of the sample with the resistor power and allowing emissions from specific phases of the burning process (e.g., only the smoldering period) to enter the chamber, we investigated a wide range of burning conditions for each fuel type. More detailed description of the samples is given in Supporting Information S1.

2.2. Chamber Experiments

To investigate the properties of both fresh and aged BB emissions, we used a 29 m^3 simulation chamber, as described in Leskinen et al. (2015). After injection of the smoke and about 15 min of mixing in the chamber, the primary emissions were characterized for about 45 min by sampling from the chamber. To initiate photochemical aging, hydrogen peroxide (H_2O_2) and ozone (O_3) were fed into the chamber and the UV lights were turned on. Dark aging was initiated by feeding only O_3 into the chamber. The target for O_3 concentration was 50 ppb for photochemical aging and 100 ppb for dark aging. To monitor the formed OH radicals during photochemical aging, a small amount of d_9-butanol was injected into the chamber. Next, the aging of the emissions was characterized for about 4.5 hr. The chamber relative humidity was set to 20%–30% for experiments with savannah originated fuels, and 40%–50% for experiments with boreal forest surface biomass to reach the daytime ambient conditions typical for these environments during the fire season.

The concentrations of CO, CO_2, and CH_4 were monitored with a Cavity Ring-Down Spectrometer (CRDS, model G2401, Picarro, Inc., USA). The O_3 concentration was monitored with a photometric analyzer (model 49i, Thermo Fisher) and the NO, NO_2, and NO_X concentrations with a chemiluminescence analyzer (model 42i, Thermo Fisher). Gas phase volatile organic compounds (including d_9-butanol) were monitored with a proton transfer reaction mass spectrometer (Vocus CI-ToF 2R with PTR reactor, abbreviated as VOCUS, Tofwerk AG, Aerodyne Inc.).

2.3. Size-Resolved CCN Measurements

Size-resolved CCN activity measurements were conducted using a CCN counter (CCNC, model CCN-100, Droplet Measurement Technologies Inc.) along with a condensation particle counter (CPC, model 3775, TSI Inc.) and a differential mobility analyzer (DMA, coaxial Vienna-type). The sample flow in the DMA was 0.8 L min^{-1} which was distributed between the CCNC (0.5 L min^{-1}) and the CPC (0.3 L min^{-1}). The sheath flow to sample flow ratio was 8:1 in the DMA and 10:1 in the CCNC.

The sample was dried with a diffusion drier and passed through a bipolar aerosol neutralizer (with ^{63}Ni source). Then, a quasi-monodisperse particle distribution was selected with the DMA. The total number concentration of this particle sample was measured using the CPC, and the number concentration of activated particles was determined by the CCNC. For each supersaturation (SS) set in the CCNC, the size in DMA was stepped from 20 to 300–600 nm, providing one full size scan in 6–10 min. The upper size limit was chosen based on the aerosol particle number size distribution in each experiment. CCN activity was measured at SS of 0.43%, 0.65%, 0.87%, and 1.1% during primary measurements. During aging, SS of 0.09%, 0.2%, and 0.31% were added and 1.1% was omitted.

The CCNC supersaturations were calibrated in the beginning and after the measurement campaign using ammonium sulfate particles (Rose et al., 2008) and comparing the results with model activation data of ammonium sulfate (Topping et al., 2016). The instrument was stable throughout the campaign.

2.4. Size Distribution Measurements

The number size distribution of the aerosol particles in the chamber was measured using a scanning mobility particle sizer (SMPS, TSI 3082 DMA + 3775 CPC). The SMPS was set to measure particles from 14.6 to 685 nm with 108 size bins. The time resolution of the SMPS measurement was 3 min.

2.5. Particle Phase Chemical Composition Characterization

The refractory BC concentration was monitored using a single-particle soot photometer (SP2, Droplet Measurement Technologies). The SP2 was calibrated on-site using size-selected Aquadag covering the size range from 70 to 400 nm. Processing the measurements, the artifact described by Schwarz et al. (2022) was accounted for. BC mass concentrations were calculated assuming a density of 1.8 g cm^{-3}.

An online high-resolution time-of-flight soot particle aerosol mass spectrometer (HR-ToF-SP-AMS, abbreviated as AMS, Aerodyne Research Inc.) was used to measure the size-resolved chemical composition and mass concentration of aerosol particles (DeCarlo et al., 2006). The instrumental operation principles and calibrations have been described in previous publications (Canagaratna et al., 2007). In this study, the AMS was operated only in EI-mode (tungsten vaporizer mode), detecting only the non-refractory material. The measurement data were averaged and saved every 2 min. The standard calibrations of ionization efficiency (IE) and relative ionisation efficiency (RIE) were performed using size-selected ammonium nitrate and ammonium sulfate particles. The RIE for ammonium and sulfate was determined to be 3.5 and 1.35, respectively. The collection efficiency (CE) was estimated by comparing the particle volume concentration calculated from the AMS data assuming a particle density of 1.25 g cm^{-3} with SMPS volume concentration measurements. The combined RIE*CE values for the organic matter during the primary emission stage were estimated to be in a range of 0.8–1.1, and those for the SOA formation stage were in a range of 0.7–0.9. The decrease in RIE*CE values during aging is due to the formation of oxidized organic components resulting in changes in particle phase state, water content, and volatility, which is consistent with observations in chamber SOA and combustion studies (Docherty et al., 2013; Lim et al., 2019). The oxygen-to-carbon (O/C) and hydrogen-to-carbon ratios (H/C) were derived using the improved ambient parametrization (Canagaratna et al., 2015).

For some experiments, a Single Particle Mass Spectrometer (SPMS) was used in addition to the AMS. The SPMS instrument (prototype of the PhotonLIZA system, Photonion GmbH) includes two reflection TOF (time-of-flight) mass analyzers and provides chemical information from both refractory and organic particle components on a single-particle level (Passig & Zimmermann, 2021). Its working principle and parameters have been described in detail previously (Schade et al., 2019). Briefly, the particles are introduced through an aerodynamic lens, detected, and sized via light scattering using a pair of continuous-wave lasers (wavelength $\lambda = 532$ nm) and photomultipliers before entering the mass spectrometer. There, the individual particles are exposed to a sequence of laser pulses to desorb and ionize both the inorganic as well as the organic particle material (Schmidt et al., 2024). The unique feature of the novel SPMS method is that in addition to inorganic compounds (salts, metals, soot) and small organic compounds (e.g., oxalate) also a molecular fingerprint of the non-polar aromatic compounds, such as the Polycyclic Aromatic Hydrocarbons (PAH), is detected on a single particle basis. Here, we focus on the ions produced by laser desorption/ionization (LDI) with 5 mJ UV pulses from a KrF excimer laser (248 nm). Mass spectra of ions of both polarities are recorded using a 14-bit digitizer (ADQ14, Teledyne SP Devices AB, Sweden) and converted into peak area with unit mass resolution using custom software. It should be noted that SPMS data do not provide quantitative mass concentrations for individual particles but can be quantified for the ensemble (Healy et al., 2013). At single-particle resolution, it reveals characteristic chemical signatures and their variations as well as information on the mixing state (Riemer et al., 2019) in comparative experiments.

2.6. Processing of CCN Data

Both the CCNC and CPC data were corrected for multiply charged particles using Wiedensohler (1988) approximation for the charge distribution. The dry activation diameter ($D50$) was calculated from the obtained

multicharge corrected CCNC and CPC data for each CCNC scan by fitting a sigmoidal function to the activated fraction ($AF(D_d) = N_{CCN}(D_d)/N_{CPC}(D_d)$) versus selected dry diameter (D_d) curve. $D50$ was determined to be the diameter for which AF was half of the AF value at the plateau of the fitted curve. The sigmoidal fits were evaluated visually, and the bad quality fits were excluded from further analysis.

The CCN activity of the particles was characterized by the hygroscopicity parameter κ introduced by Petters and Kreidenweis (2007). The so-called κ-Köhler theory defines the saturation ratio over a droplet with curvature as

$$S(D) = \frac{D^3 - D_d^3}{D^3 - D_d^3(1-\kappa)} \exp\left(\frac{4\sigma_{s/a}M_w}{RT\rho_w D}\right), \quad (1)$$

where D is the diameter of the droplet, D_d is the diameter of the dry particle, $\sigma_{s/a}$ is the surface tension of the droplet at the solution/air interface, M_w is the molecular weight of water, R is the universal gas constant, ρ_w is the density of water and T is the temperature. Values of κ were determined iteratively from the κ-Köhler theory (Equation 1) by using $D50$ as the value for D_d and finding the κ value that yields the Köhler curve with a maximum at the SS corresponding to the chosen $D50$ value. Measurement uncertainty for SS (ΔSS) was defined as the standard error of the Deming regression (Hall, 2022) estimate for the linear fit obtained in SS calibration. The uncertainty in $D50$ ($\Delta D50$) was defined to be the size bin width or the 95% confidence bound of the sigmoidal fit, depending on which of the two was smaller. Both the uncertainty in SS and $D50$ was considered when calculating the uncertainty in κ using the combination of $D50 + \Delta D50$ and SS + ΔSS as the lower bound and $D50 - \Delta D50$ and SS − ΔSS for the upper bound.

2.7. Modified Combustion Efficiency

To characterize the burning condition, the average modified combustion efficiency (MCE) was determined for each experiment. MCE was calculated with the CO and CO_2 concentrations measured with the CRDS in the diluted smoke fed into the chamber. MCE was calculated as:

$$\mathrm{MCE} = \frac{\Delta CO_2}{\Delta CO_2 + \Delta CO}, \quad (2)$$

where ΔCO_2 and ΔCO are the concentrations of carbon dioxide and carbon monoxide with the effect of the room and dilution air removed (Ward & Radke, 1993). It should be noted that, the time resolution of the CRDS (5 s) is relatively low compared to fast changes in smoke characteristics. This may have caused fast peaks in CO and CO_2 concentrations to go unnoticed, introducing additional uncertainty. Pure smoldering corresponds to an MCE value of 0.8 or less, and pure flaming to an MCE value of ~0.99 (Yokelson et al., 1996). Equal amount of smoldering and flaming corresponds to an MCE of 0.9.

2.8. CCN Emission Factors

Emission factors define the amount (e.g., mass or number) of a pollutant, such as CCN, emitted per unit mass of burned biomass. CCN emission factors (EF_{CCN}) were determined for primary emissions with the carbon mass balance method (Ward & Radke, 1993; Yokelson et al., 1999). EF_{CCN} was calculated based on the CCN number concentrations in the chamber and therefore is representative only of the burning conditions chosen to be investigated in each experiment. CCN emission factors (in # (kg fuel)$^{-1}$) were calculated as

$$EF_{CCN} = F_C \cdot 1000 \cdot \frac{ER_{CCN}}{\frac{\sum C}{\Delta CO}}, \quad (3)$$

where F_C is fuel carbon mass fraction, ER_{CCN} is the emission ratio of CCN (in g^{-1}) and the summation $\sum C$ includes carbon in ΔCO_2, ΔCO, and ΔCH_4 from the CRDS measurements during the chamber feed with effect of the room and dilution air removed as well as carbon in volatile organic compounds measured with VOCUS, and particle phase carbon measured with AMS and SP2. ER_{CCN} is calculated as

Table 1
Summary of Experiments With CCN Measurements During the BASFAA Campaign Including Fuel Type, Modified Combustion Efficiency (MCE), and Aging Type

Date	Fuel type	MCE	Aging
16 May 2022	Savannah grass	0.952 (±0.001)	OH
17 May 2022	Savannah wood	0.589 (±0.055)	OH
19 May 2022	Savannah wood	0.886 (±0.003)	OH
20 May 2022	Savannah wood	0.858 (±0.005)	OH
23 May 2022	Savannah wood	0.929 (±0.001)	OH
24 May 2022	Savannah wood	0.935 (±0.001)	OH
25 May 2022	Boreal forest surface	0.763 (±0.009)	OH
27 May 2022	Boreal forest surface	0.741 (±0.012)	OH
30 May 2022	Boreal forest surface	0.702 (±0.015)	OH
31 May 2022	Savannah wood	0.672 (±0.022)	Dark
1 June 2022	Savannah wood	0.950 (±0.001)	Dark
2 June 2022	Savannah wood	0.892 (±0.002)	Dark
3 June 2022	Savannah grass	0.843 (±0.002)	Dark
6 June 2022	Savannah grass	0.973 (±0.0004)	OH
7 June 2022	Savannah grass	0.895 (±0.002)	OH
8 June 2022	Boreal forest surface	0.743 (±0.006)	Dark
9 June 2022	Boreal forest surface	0.839 (±0.003)	OH
10 June 2022	Boreal forest surface	0.758 (±0.009)	Dark

$$\mathrm{ER_{CCN}} = \frac{N_{\mathrm{CCN}}}{\frac{M_C \cdot P}{R \cdot T} \cdot 10^{-6} \cdot \Delta \mathrm{CO_{chamber}}}, \quad (4)$$

where N_{CCN} is the number concentration of CCN particles (in $\mathrm{m^{-3}}$) calculated from the SMPS size distribution as the sum of particles larger than $D50$ (SS = 0.43%), M_C is the molar mass of carbon, P is pressure, R is the universal gas constant, T is temperature and $\Delta \mathrm{CO_{chamber}}$ is the concentration of CO in the chamber (in ppm) with the chamber background subtracted.

3. Results and Discussion

CCN data were recorded during 18 combustion experiments, of which eight were conducted with savannah wood, four with savannah grass, and six with boreal forest surface material (Table 1). Due to bimodal size distribution, we could not determine a single κ value for the primary aerosol in experiment on 2 June and for the aged aerosol in experiments on 27 and 30 May as well as 2 June. These data have been excluded from the CCN analysis. Relatively low MCE values were observed for the combustion of boreal forest surface material ranging from 0.74 to 0.84. These MCE values correspond to pure smoldering and smoldering dominated burning conditions. Contrary to boreal forest surface, relatively high MCE values (0.84–0.97) were observed with savannah grass, corresponding to smoldering-dominated and flaming-dominated burning conditions. For savannah wood combustion, the widest MCE range was observed with MCE values ranging from 0.59 to 0.95. Field measurements of the African savannah and grassland burning emissions suggest that flaming is the more dominant burning condition in such fires, with average MCE varying from 0.94 to 0.97 (Abdulraheem et al., 2020; Andreae, 2019; Sinha et al., 2003), though there may be seasonal changes (Vernooij et al., 2023). Smoldering appears to be slightly more dominant in boreal forest fires with an average MCE of 0.88 (McRae et al., 2006). Considering this, we were able to achieve the average MCE values for savannah fires but did not reach the average values for boreal forest surface fires.

3.1. Hygroscopicity of Primary Particles

CCN activity of the primary particles was measured for about 45 min after the chamber filling and the 15-min mixing period. During the primary measurement, the particle phase composition was stable in most of the experiments as indicated by the elemental composition derived from the AMS measurement (see Figure S1 in Supporting Information S1). In high MCE experiments with savannah wood, there is a slight decrease in the mass fraction of organics and a slight increase in the mass fraction of NO_3. The hygroscopicity parameter κ was calculated for several supersaturations (SS) from 0.2% to 0.87%; however, the best coverage of data over all experiments was recorded with SS of 0.43%. Hence, the data with this SS will be used throughout this study. The trends in κ with increasing MCE were similar between the different SS; however, within the same MCE, the different SS resulted in slightly different κ values (see Figure S2 in Supporting Information S1).

First, we investigate how the hygroscopicity of the primary BB particles depends on the burning condition (i.e., MCE) and the burned biomass type. Figure 1 presents the measured κ values (SS = 0.43%) for primary emissions of all BB experiments as a function of MCE. In all experiments, primary aerosol had low to moderate hygroscopicity with κ values ranging from 0.07 to 0.19 (Figure 1). In experiments with savannah wood and boreal forest surface material (i.e., the biomasses for which the low MCE was achieved) with MCE < 0.84, the particle hygroscopicity was observed to be quite independent of MCE with mean κ of 0.079 (standard deviation = 0.007). The hygroscopicity of the savannah wood and grass burning particles showed an increasing trend with MCE within the experiments having MCE above 0.84. Therefore, we found that flaming-dominated burning of savannah wood produced particles with higher hygroscopicity compared with smoldering-dominated burning. Due to the lack of measurements with high MCE for boreal forest surface material and low MCE for savannah grass, we are not able to compare the trends for the different biomass types over the wide MCE range. Namely, we

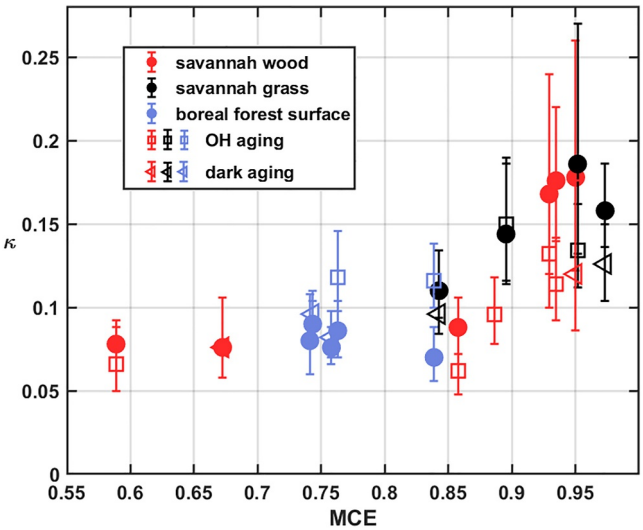

Figure 1. Hygroscopicity of primary and aged particles as a function of modified combustion efficiency (MCE) for supersaturation of 0.43%. Filled circles correspond to primary aerosol. Open squares indicate photochemically aged aerosol and open triangles indicate dark aged aerosol. Error bars show the uncertainty in supersaturation and activation diameter reflected in κ.

cannot predict if particles from boreal forest surface burning would also exhibit increasing κ values in flaming-dominated burning conditions.

The observed κ values are within the same range as reported in other studies with BB aerosol. Petters et al. (2009) observed similar BB aerosol hygroscopicity ($0.05 < \kappa < 0.19$) for fuels containing for example needles, branches and leaves from various tree species; however, the whole range of observed hygroscopicity was much broader than in our measurements. Carrico et al. (2010) reported κ values of around 0.1 derived from H-TDMA data for particles emitted in burning of some boreal fuels in smoldering conditions. Li (2019) measured the hygroscopicity of sawgrass burning particles and obtained κ values of ~0.21 for fresh particles dominated with organic material.

3.2. Hygroscopicity of Aged Particles

After the primary CCN measurements, aging was initiated in the chamber, and the hygroscopicity of the aging aerosol particles was monitored for about 4.5 hr. At the end of the photochemical experiments, OH exposure ranged from 8.3×10^{10} to 15.7×10^{10} molecules cm^{-3} s which corresponds to an equivalent photochemical age of 0.6–1.2 days (assuming 24-hr average ambient [OH] = 1.5×10^6 molecules cm^{-3} (Mao et al., 2009)). Similarly, at the end of dark aging, the O_3 exposure ranged from 3.7×10^{16} to 4.7×10^{16} molecules cm^{-3} s, corresponding to equivalent atmospheric age of 0.6–0.8 days (assuming 24-hr average ambient [O_3] = 7×10^{11} molecules cm^{-3} (Atkinson & Arey, 2003)). Here, we present the hygroscopicity of the photochemically and dark-aged particles toward the end of aging for 0.43% SS. Figure 1 presents the hygroscopicity of the aged BB particles as a function of MCE. Data points with similar OH exposure (8.0×10^{10}–11.2×10^{10} molecules cm^{-3} s, equivalent atmospheric age of 14.7–20.8 hr) were chosen for photochemical experiments. For dark aging, the last data point of each experiment was chosen.

In most experiments, the most significant changes in hygroscopicity occurred during the first hour of aging. Three exemplary time series of κ can be seen in Figure 2. The measured κ values of the photoaged aerosol varied from 0.07 to 0.15 and for the dark aged from 0.08 to 0.13 at 0.43% SS. The direction of the change in κ was similar for all SS, but the magnitude of the change varied (see Figure S2 in Supporting Information S1). Photochemical aging resulted in an increase in the particle hygroscopicity in the low MCE (<0.84) experiments with boreal forest surface material, while dark aging had only a minor effect. In the two savannah wood experiments with low MCE, dark aging had no effect on hygroscopicity, while photochemical aging resulted in a slight decrease in kappa. A clear decrease in hygroscopicity was observed in most of the experiments with high MCE (>0.84) both during the dark and photochemical aging. In other words, an increase or no change in hygroscopicity was observed for particles with low initial hygroscopicity and a decrease in hygroscopicity was observed for particles with higher initial hygroscopicity. This is surprising as the oxidation state of the organic fraction increased during the oxidation process in all the experiments (see Figure S3 in Supporting Information S1), which is typically associated with an increase in observed hygroscopicity (Jimenez et al., 2009). Similar to us, Engelhart et al. (2012) reported a decrease in κ for particles with high initial hygroscopicity and vice versa, causing the overall variability in hygroscopicity to decrease. Based on our results, the burning condition (represented by MCE) seems to be an important factor affecting the change in particle hygroscopicity during aging.

3.3. Chemical Composition and Links to Particle Hygroscopicity

To better understand the dependency of hygroscopicity on MCE and the changes in κ during the oxidation process, we investigate the chemical composition of both primary and aged aerosol. The chemical composition of the aerosol was characterized with an AMS and an SPMS, and the black carbon (BC) concentration with an SP2. In this section, we present the aerosol composition as measured from the chamber for 1 hr before aging started and at the end of aging. In these two experimental stages, we examined the size-resolved chemical composition of

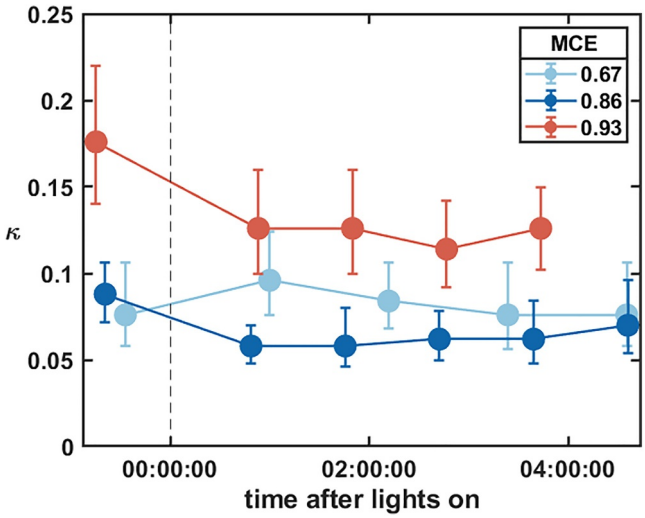

Figure 2. Time series of hygroscopicity parameter κ for supersaturation of 0.43% during three exemplary savannah wood experiments with photochemical aging (MCE = 0.86, 0.93) and dark aging (MCE = 0.67). The vertical dashed line marks the start of aging. The solid lines are shown only to guide the eye.

aerosol particles across all the size ranges. We observed that the chemical composition of smaller particles (e.g., 80 nm) was very similar to that of large particles (e.g., 300 nm).

Based on the measurements with the AMS and the SP2, the organic material highly dominated the total mass of non-refractory material and BC, having a mass fraction of 86%–99% (Figure 3). This was observed for both primary and aged particles in all fuel types and burning conditions. Both non-refractory inorganic materials (including ammonium nitrate, ammonium sulfate, ammonium bisulphate, and sulfuric acid) and BC remained low in all experiments with mass fractions of 0.4%–6% and 0%–8.1%, respectively. These results are consistent with several field and laboratory studies reporting high organic fractions and low elemental carbon (EC) (or BC) fractions in wildfire emissions with MCE < 0.97 (Christian et al., 2003; Hosseini et al., 2013; Liang et al., 2022; Pokhrel et al., 2016). Very low and almost constant EC/OC values at MCE < 0.97 were reported by Pokhrel et al. (2016), also in line with our observations. We see a small increase in the BC/OC ratio at the highest MCE values (see Figure 3); however, we did not achieve the burning conditions where this ratio is expected to increase strongly (Pokhrel et al., 2016).

The observed relatively low hygroscopicity of the primary aerosol in experiments with MCE < 0.84 is consistent with previously published values for primary BB emissions (Petters et al., 2009), and with the high organic fraction and low carbon oxidation state (OSc) as measured with the AMS. However, when using a simple mixing rule and the literature values of κ for BC and different organic and inorganic chemical components analyzed by AMS, the slight decrease of the organic and increase of the inorganic fractions are not sufficient to explain the higher hygroscopicity of the primary aerosol in the experiments with high MCE. The hygroscopicity of the primary particles is shown in Figure 4 as a function of OSc, which can be used to estimate the degree of oxygenation of the aerosol particles (OSc = 2*O/C-H/C, Kroll et al., 2011). There were clear differences in OSc between the burned biomass types. Primary particles emitted during BB of boreal forest surface material appear to be less oxidized with OSc from −1.5 to −1.2 compared to savannah wood (−1.2 < OSc < −0.9) and savannah grass (−0.7 < OSc < −0.5). When the whole data set is considered, there is a moderate positive correlation of κ with increasing OSc (R^2 = 0.50 for SS of 0.43%), but within the different biomass types, the trend is not always clear. In the case of savannah wood, there is a large scatter in κ and no increasing trend with increasing OSc can be seen. Hence, the differences in primary aerosol hygroscopicity cannot be fully explained by differences in OSc.

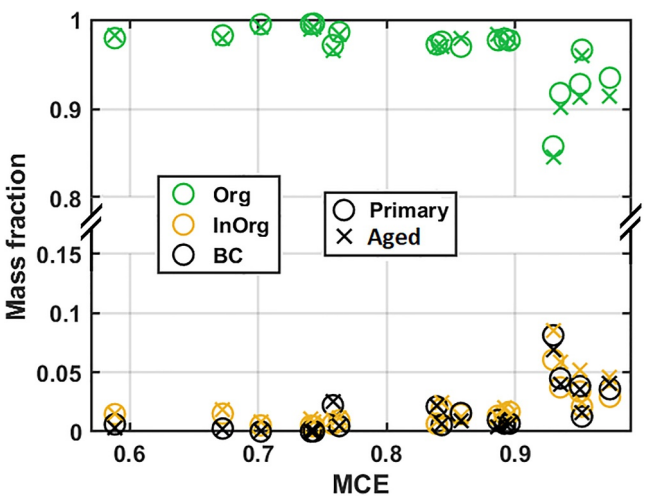

Figure 3. Mass fractions of organic and inorganic material (as measured with the AMS) as well as black carbon (BC) in primary and aged particles as a function of MCE. Mass fractions for primary aerosol are shown with open circles and for aged aerosol with crosses.

During photochemical aging, SOA formation was observed in most of the experiments. However, the mass fractions of total organic material, inorganic material, and BC did not change notably as the initial organic fraction was already close to 1 (Figure 3). During all experiments with photochemical aging, the O/C ratio increased with time while the H/C ratio decreased, resulting in an increase in OSc (see Figures S3 and S4 in Supporting Information S1). In these experiments, OSc increased rapidly during the first hour of aging and continued to increase more slowly until the end of the experiment. A slight increase in OSc was observed in most of the dark aging experiments (see Figures S5 and S6 in Supporting Information S1). These changes in OSc are consistent with the observed changes in κ in experiments with boreal forest surface material. However, the increase in OSc during photochemical aging, and the minor changes in organic and inorganic fractions seem to be contradictory to the observed decrease in hygroscopicity with ongoing oxidation in experiments with MCE > 0.84 (see Figure 1). Hygroscopicity of the particles can also be affected by many other physicochemical properties of organic aerosols that are not detectable by the AMS. Characteristics of organic aerosol, such as water solubility and molecular mass (Han

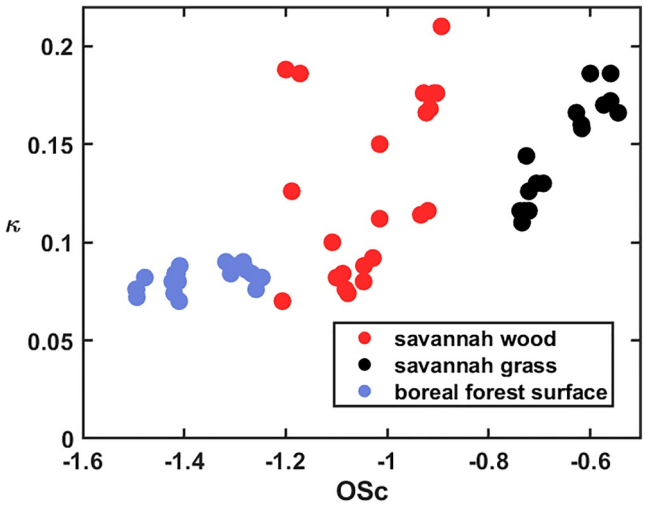

Figure 4. Hygroscopicity parameter κ versus the mean carbon oxidation state (OSc) for all supersaturations during the primary measurements.

et al., 2022), may differ between the experiments and change during aging, contributing to the change in κ. However, based on our calculations, these changes cannot fully explain the changes in κ during aging.

The seemingly contradicting behavior of hygroscopicity with particle composition based on AMS and SP2 measurements indicates that, most likely, we were not able to detect all chemical constituents of the BB aerosol with these methods. Previous studies have reported that inorganic and organic salts, not quantitatively detected by AMS, may form a significant fraction of BB emissions (Corbin et al., 2015; Haslett et al., 2018), and therefore influence their physico-chemical properties. Many of these salts, such as KCl and K_2SO_4, are very hygroscopic (κ = 0.99 and κ = 0.55, respectively), substantially increasing the κ value even if they are not the dominant fraction. With its ability to detect metals (Passig et al., 2020) and a range of organic species on a single-particle basis (Passig et al., 2022), SPMS can be used as a complement to more common online MS technologies, filling in some of the gaps left by analysis with, for example, AMS. Here, we use the obtained SPMS spectra as a qualitative indicator to identify compounds and trends in the composition that could explain the observed differences in hygroscopicity. Due to the complex ionisation mechanisms, it is difficult to quantify the aerosol chemical composition from the signals in SPMS mass spectra without thorough calibration, but the relative changes upon aging or between sources can be reliably determined.

Figure 5 shows the average particle mass spectra for one example case for each of the three fuels studied, showing both the primary emissions and the emissions at the end of the aging process. Each spectrum represents the sum of 2,500 single-particle mass spectra, irrespective of particle size. The mass spectra of primary emissions from boreal forest surface material (Figure 5a, top) reveal a high content of organic material, including fragments of organic nitrogen species from biomass pyrolysis (CN^- and CNO^-) and comparably strong signals from oxygen-

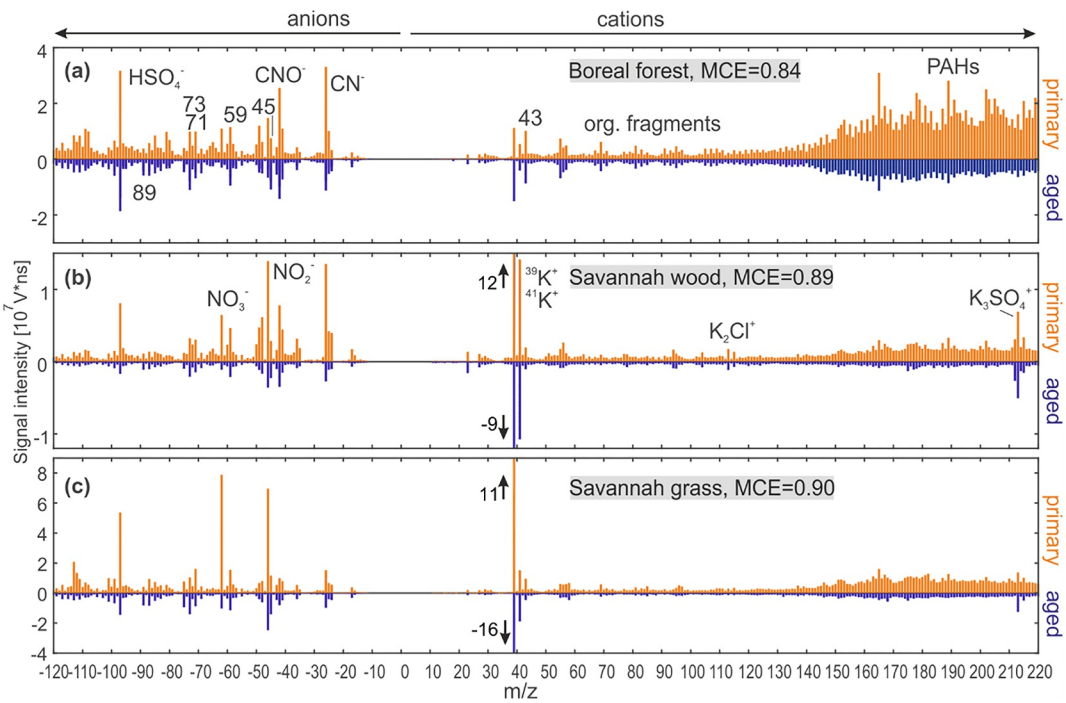

Figure 5. Summed SPMS bipolar mass spectra (each n = 2,500) from primary particles (top) and from particles sampled during the end of photochemical aging (bottom). (a) Particles from the boreal forest surface (9 June), (b) particles from savannah wood material (19 May), and (c) particles from savannah grass material (7 June). Note that in SPMS, the peak area is not a direct measure of the mass concentration values without thorough calibration.

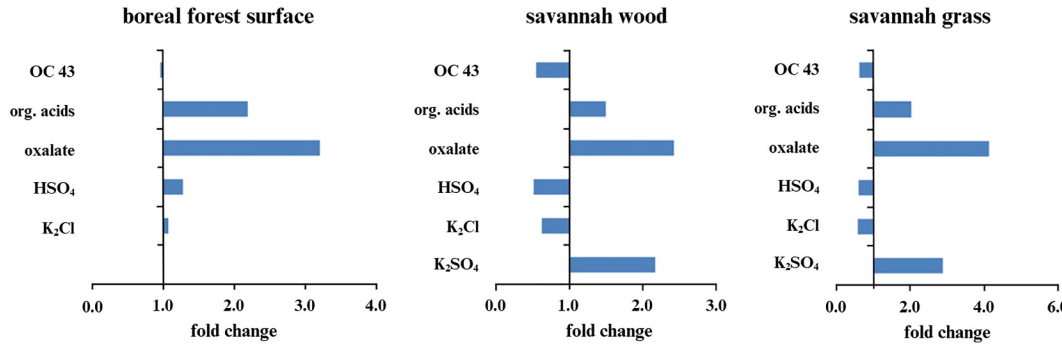

Figure 6. Changes in relative peak area (RPA) with photochemical aging for selected compounds from the same particles as in Figure 5. In boreal forest particles, the $K_2SO_4^+$ signal is strongly overlaid by organic fragments. OC 43 indicates $m/z = +43$, a peak made by both oxygen-containing and non-oxygen containing fragments; organic acids include the sum of $m/z = -73, -71, -59, -45$.

containing organic carbon (OC) ($C_2H_3O^+$) and organic acids (HCO_2^-, $CH_3CO_2^-$, $C_2H_3CO_2^-$, and $C_2HO_3^-$) (Zauscher et al., 2013; Zhang et al., 2017). After about 4.5 hr of photoaging, the signal of many OC fragments and polycyclic aromatic hydrocarbons decreased, whereas organic acids remained stable. The potassium signal increases, probably due to the loss of masking organic coatings (Zauscher et al., 2013). Further aging effects are illustrated by the changes in relative peak areas (RPA), defined as the normalized peak area of one m/z channel to the total ion intensity (see Figure 6). The increase in the peak at $m/z = -89$ reflects the formation of oxalate in BB particles (Srivastava et al., 2019; Zhang et al., 2017). The observed changes in OC composition toward higher oxidized, more water-soluble organics are consistent with the increase in oxidation state derived from AMS data (Figure S3 in Supporting Information S1) and with the moderate increase in hygroscopicity (Figure 1).

In contrast to the boreal forest surface biomass, the savannah wood and grass particle mass spectra are characterized by strong potassium signals (Figures 5b and 5c). Prominent potassium signals are a typical feature in SPMS due to its low ionization potential (Reinard & Johnston, 2008). Therefore, OC can still be the dominant mass fraction, especially at low MCE values, and the hygroscopicity, in this case, is comparable to boreal forest material (Figure 1). But the clear difference in the dominance of the potassium signal between savannah biomasses and the boreal forest surface material is a strong indication that the potassium contents of these samples are different. These differences in the potassium signal are also visible in the AMS data. Although SPMS data is not available for all experiments, it is reasonable that the relative fraction of inorganic particle constituents increases with higher MCE values, resulting in higher κ values. A qualitative explanation for the observed decrease in hygroscopicity with aging in experiments with savannah wood and grass can be found in the chemistry of potassium salts. Heterogeneous reactions converting potassium chloride via potassium nitrate to potassium sulfate are documented for the aging process of BB organic aerosol and are associated with changes in deliquescence and a decrease in hygroscopicity (Freney et al., 2009; Li et al., 2003). In line with this, the SPMS data shows a decrease in the RPA of K_2Cl^+ and HSO_4^- as well as an increase of $K_3SO_4^+$ (see Figures 6b and 6c).

Beyond the potassium salts, the formation of organic salts can substantially affect the hygroscopicity of internally mixed particles (Drozd et al., 2014). In particular, the presence of oxalic acid has been reported to reduce the hygroscopicity by the formation of less water-soluble potassium oxalate (Boreddy et al., 2014; Jing et al., 2017), but also mixtures with levoglucosan revealed similar trends (Jing et al., 2017). While the resulting organic salts are likely to fragment in the ionization process of the SPMS, the presence of oxalate and organic acids, and the observed decrease of the K_2Cl^+ signal are consistent with this transformation and can contribute to the observed decrease in hygroscopicity during aging of the BB emissions from savannah materials.

3.4. CCN Emission Factors

CCN emission factors (EF_{CCN}) for supersaturation of 0.43%, derived from SMPS size distributions and CCN activation diameters ($D50$) for primary aerosol, are presented in Figure 7. The primary size distributions, averaged over the time of the CCN measurement, and the $D50$ values are shown in Figure S7 of the Supporting Information S1. The uncertainty due to the minimal changes in the size distribution (e.g., due to wall losses or

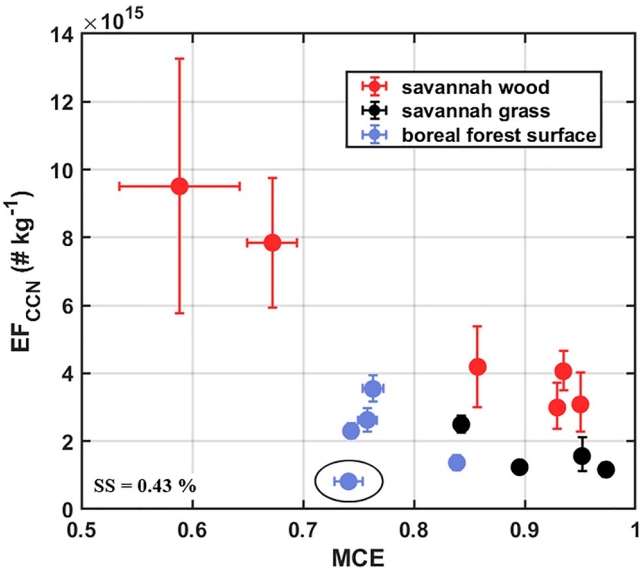

Figure 7. CCN emission factors as the number of emitted CCN per kg of burned biomass as a function of MCE for supersaturation (SS) of 0.43%. Error bars represent the measurement uncertainties for EF_{CCN} and MCE. If error bars are not visible, they are smaller than the size of the marker. The circled experiment with boreal forest surface material included only the emissions from smoldering phase prior to flame ignition, while the other boreal forest surface experiments included emissions from the flaming phase as well as the smoldering phases before and after the flame. All other experiments included emissions from both the smoldering and flaming phases.

coagulation) over the primary measurement phase falls within the measurement uncertainty. For boreal forest surface, EF_{CCN} varies from 0.8×10^{15} to 3.5×10^{15} (kg fuel)$^{-1}$ at a SS of 0.43%, and for savannah wood and savannah grass from 3.0×10^{15} to 9.5×10^{15} (kg fuel)$^{-1}$ and 1.2×10^{15} to 2.5×10^{15} (kg fuel)$^{-1}$, respectively. Our values for boreal forest surface are similar to the previously published EF_{CCN} value of 1.6×10^{15} (kg fuel)$^{-1}$ (SS = 0.5%) for boreal forest fire by Andreae (2019). For savannah and grassland fires, the previously published values are close to our results for savannah grass material at high MCE. For these types of fires, Andreae (2019) reported EF_{CCN} value of 7.9×10^{14} (kg fuel)$^{-1}$ for SS of 0.5%; however, burning condition was not specified. Emission factors for particles larger than 100 nm (often used estimate for *D*50) were published by Janhäll et al. (2010) for savannah and grassland fires and ranged from 2.1×10^{14} (kg fuel)$^{-1}$ to 6.6×10^{14} (kg fuel)$^{-1}$. These fires were characterized with MCE values typical for flaming dominated burning ($0.95 < MCE < 0.98$). In our data, a decreasing trend with increasing MCE can be seen within experiments with savannah wood and grass material, similar to previous observations by Janhäll et al. (2010). In the case of boreal forest surface, the scatter in EF_{CCN} is large and there is no clear trend with MCE. In Figure 7, the circled experiment included only smoldering emissions before visible flames appeared, while in the other experiments of boreal forest surface material, emissions from the flaming phase as well as the smoldering phases before and after the flame were included. Comparing these two types of experiments with similar MCE, we can see that the EF_{CCN} is smaller in the experiment with only the smoldering part compared to the experiments where emissions from the whole combustion were included.

It should be noted that even if the EF_{CCN} is the highest at low MCE, the overall emissions of CCN from BB are more complex to determine. For example, in boreal forest fires where a large amount of moist biomass is burned, the duration of the smoldering phase can be much longer than the duration of the flaming phase with high MCE. At the same time, the amount of the burned biomass is significantly higher during the flaming phase (Wang et al., 2021), which may result in larger overall emissions from the flaming phase compared to the smoldering one.

4. Conclusions

In this study, we characterized the hygroscopicity of aerosol particles emitted during open laboratory combustion of woody and grassy material from the South African savannah as well as surface material from a Finnish boreal forest. We have evaluated the effects of burning conditions and fuel type as well as photochemical and dark aging on the hygroscopicity of the particles. Our results suggest that primary particles from flaming combustion are more hygroscopic compared with those from smoldering combustion. This is possibly due to the larger contribution of inorganic material, such as potassium-containing salts to the chemical composition of flaming particles as suggested by the qualitative analysis of SPMS data. During both photochemical and dark aging, the variability in hygroscopicity between different burning conditions decreased, and the hygroscopicity parameter κ seemed to approach the value of 0.1. The increased hygroscopicity in the experiments with smoldering combustion was driven by the increase in the oxidation state of the organic fraction. The observed decrease in the experiments with flaming-dominated combustion was likely due to changes in the refractory inorganic fraction toward less hygroscopic compounds.

Due to the lack of smoldering experiments with savannah grass and flaming experiments with boreal forest surface material, we cannot conclude whether there are differences in hygroscopicity between the biomass types over the entire MCE range. Therefore, more data are needed to determine whether the fuel type or the burning condition is a more important factor in determining the hygroscopicity of the BB aerosol for these fuels. However, within the available data, we did not observe clear differences in κ between smoldering of savannah wood and boreal forest surface and more flaming dominated burning of savannah wood and savannah grass. Our findings,

even if not complete, highlight the importance of characterizing the burning condition when reporting the properties of BB aerosols.

Chemical composition is sometimes used as a proxy for hygroscopicity by using literature values of κ and mass fractions measured with, for example, an AMS. As our results show, non-refractory composition measured with AMS fails to capture all the constituents, especially the refractory inorganic compounds in aerosol particles from flaming combustion, possibly underestimating the κ values. For this reason, it is important to also consider the refractory material of BB aerosol when calculating κ from chemical composition.

In addition to hygroscopicity, we determined the primary CCN emission factors, indicating the number of CCN active particles in the fresh smoke for each kilogram of burned fuel, at supersaturation of 0.43%. Contrary to the hygroscopicity, we observed differences in EF_{CCN} between the fuels. A decreasing trend with increasing MCE was observed for EF_{CCN} with the savannah-originated fuels, as expected. EF_{CCN} was lower for BB of savannah grass compared to BB of savannah wood in similar burning conditions. In the case of boreal forest surface experiments, the data are more scattered. It should be noted that due to changes in particle hygroscopicity and aerosol size distribution during the aging as well as the large variability in the supersaturation conditions in the atmosphere, the overall number of CCN originating from BB is much more complex.

Overall, our results provide a new understanding of the effects of biomass type, burning condition, and atmospheric aging on BB particle hygroscopicity and CCN emission factors. Our results highlight the importance of taking the burning condition into account when characterizing the hygroscopicity of BB aerosol. This is especially important for primary aerosols where the differences in hygroscopicity are pronounced. For long-range transported aerosols that have undergone changes in the atmosphere due to photochemical and/or dark aging, the differences in hygroscopicity may be smaller. Future studies are needed to further investigate the differences in hygroscopicity and EF_{CCN} between the studied fuels over a wide MCE range.

Conflict of Interest

The authors declare no conflicts of interest relevant to this study.

Data Availability Statement

The data used in this study are available at Peltokorpi et al. (2025).

Acknowledgments
This project was supported by the Research Council of Finland (Grants 337550, 343359) and by the European Commission under the Horizon 2020—Research and Innovation Framework Programme, H2020-INFRAIA-2020-1, Grant Agreement number: 101008004. Furthermore, EIR, JP, and RZ gratefully acknowledge support from the Helmholtz Association in the framework of the "aeroHEALTH" Helmholtz International Lab, and funding by the Deutsche Forschungsgemeinschaft (DFG, German Research Foundation)—SFB 1477 "Light-Matter Interactions at Interfaces", project number 441234705. HL acknowledges the financial support of Centre of Excellence Programme (decision no. 374082 and 374081). Open access publishing facilitated by Ita-Suomen yliopisto, as part of the Wiley - FinELib agreement.

References

Abdulraheem, K. A., Adeniran, J. A., Aremu, A. S., Yusuf, M.-N. O., Adebisi, J. A., Sadiku, N. A., et al. (2020). Emission factors of some common grass species in West Africa. *Environmental Monitoring and Assessment*, *192*(12), 758. https://doi.org/10.1007/s10661-020-08725-0

Andreae, M. O. (2019). Emission of trace gases and aerosols from biomass burning—An updated assessment. *Atmospheric Chemistry and Physics*, *19*(13), 8523–8546. https://doi.org/10.5194/acp-19-8523-2019

Atkinson, R., & Arey, J. (2003). Atmospheric degradation of volatile organic compounds. *Chemical Reviews*, *103*(12), 4605–4638. https://doi.org/10.1021/cr0206420

Bellouin, N., Boucher, O., Haywood, J., & Reddy, M. (2005). Global estimate of aerosol direct radiative forcing from satellite measurements. *Nature*, *438*(7071), 1138–1141. https://doi.org/10.1038/nature04348

Boreddy, S. K. R., Kawamura, K., Mkoma, S., & Fu, P. (2014). Hygroscopic behavior of water-soluble matter extracted from biomass burning aerosols collected at a rural site in Tanzania, East Africa. *Journal of Geophysical Research: Atmospheres*, *119*(21), 12233–12245. https://doi.org/10.1002/2014JD021546

Canagaratna, M. R., Jayne, J. T., Jimenez, J. L., Allan, J. D., Alfarra, M. R., Zhang, Q., et al. (2007). Chemical and microphysical characterization of ambient aerosols with the aerodyne aerosol mass spectrometer. *Mass Spectrometry Reviews*, *26*(2), 185–222. https://doi.org/10.1002/mas.20115

Canagaratna, M. R., Jimenez, J. L., Kroll, J. H., Chen, Q., Kessler, S. H., Massoli, P., et al. (2015). Elemental ratio measurements of organic compounds using aerosol mass spectrometry: Characterization, improved calibration, and implications. *Atmospheric Chemistry and Physics*, *15*(1), 253–272. https://doi.org/10.5194/acp-15-253-2015

Carrico, C. M., Petters, M. D., Kreidenweis, S. M., Sullivan, A. P., McMeeking, G. R., Levin, E. J. T., et al. (2010). Water uptake and chemical composition of fresh aerosols generated in open burning of biomass. *Atmospheric Chemistry and Physics*, *10*(11), 5165–5178. https://doi.org/10.5194/acp-10-5165-2010

Che, H., Segal-Rozenhaimer, M., Zhang, L., Dang, C., Zuidema, P., Dobracki, A., et al. (2022). Cloud processing and weeklong ageing affect biomass burning aerosol properties over the south-eastern Atlantic. *Communications Earth & Environment*, *3*(1), 1–9. https://doi.org/10.1038/s43247-022-00517-3

Ching, J., Fast, J., West, M., & Riemer, N. (2017). Metrics to quantify the importance of mixing state for CCN activity. *Atmospheric Chemistry and Physics*, *17*(12), 7445–7458. https://doi.org/10.5194/acp-17-7445-2017

Christian, T. J., Kleiss, B., Yokelson, R. J., Holzinger, R., Crutzen, P. J., Hao, W. M., et al. (2003). Comprehensive laboratory measurements of biomass-burning emissions: 1. Emissions from Indonesian, African, and other fuels. *Journal of Geophysical Research*, *108*(D23), 4719. https://doi.org/10.1029/2003JD003704

Corbin, J., Lohmann, U., Sierau, B., Keller, A., Burtscher, H., & Mensah, A. A. (2015). Black carbon surface oxidation and organic composition of beech-wood soot aerosols. *Atmospheric Chemistry and Physics*, *15*(20), 11885–11907. https://doi.org/10.5194/acp-15-11885-2015

Damoah, R., Spichtinger, N., Forster, C., James, P., Mattis, I., Wandinger, U., et al. (2004). Around the world in 17 days—Hemispheric-scale transport of forest fire smoke from Russia in May 2003. *Atmospheric Chemistry and Physics*, *4*(5), 1311–1321. https://doi.org/10.5194/acp-4-1311-2004

DeCarlo, P. F., Kimmel, J. R., Trimborn, A., Northway, M. J., Jayne, J. T., Aiken, A. C., et al. (2006). Field-deployable, high-resolution, time-of-flight aerosol mass spectrometer. *Analytical Chemistry*, *78*(24), 8281–8289. https://doi.org/10.1021/ac061249n

Descals, A., Gaveau, D. L. A., Verger, A., Sheil, D., Naito, D., & Peñuelas, J. (2022). Unprecedented fire activity above the Arctic Circle linked to rising temperatures. *Science*, *378*(6619), 532–537. https://doi.org/10.1126/science.abn9768

Docherty, K. S., Jaoui, M., Corse, E., Jimenez, J. L., Offenberg, J. H., Lewandowski, M., & Kleindienst, T. E. (2013). Collection efficiency of the aerosol mass spectrometer for chamber-generated secondary organic aerosols. *Aerosol Science and Technology*, *47*(3), 294–309. https://doi.org/10.1080/02786826.2012.752572

Drozd, G., Woo, J., Häkkinen, S. A. K., Nenes, A., & McNeill, V. F. (2014). Inorganic salts interact with oxalic acid in submicron particles to form material with low hygroscopicity and volatility. *Atmospheric Chemistry and Physics*, *14*(10), 5205–5215. https://doi.org/10.5194/acp-14-5205-2014

Dusek, U., Frank, G. P., Massling, A., Zeromskiene, K., Iinuma, Y., Schmid, O., et al. (2011). Water uptake by biomass burning aerosol at sub- and supersaturated conditions: Closure studies and implications for the role of organics. *Atmospheric Chemistry and Physics*, *11*(18), 9519–9532. https://doi.org/10.5194/acp-11-9519-2011

Engelhart, G. J., Hennigan, C. J., Miracolo, M. A., Robinson, A. L., & Pandis, S. N. (2012). Cloud condensation nuclei activity of fresh primary and aged biomass burning aerosol. *Atmospheric Chemistry and Physics*, *12*(15), 7285–7293. https://doi.org/10.5194/acp-12-7285-2012

Farley, R., Bernays, N., Jaffe, D. A., Ketcherside, D., Hu, L., Zhou, S., et al. (2022). Persistent influence of wildfire emissions in the Western United States and characteristics of aged biomass burning organic aerosols under clean air conditions. *Environmental Science & Technology*, *56*(6), 3645–3657. https://doi.org/10.1021/acs.est.1c07301

Freney, E. J., Martin, S. T., & Buseck, P. R. (2009). Deliquescence and efflorescence of potassium salts relevant to biomass-burning aerosol particles. *Aerosol Science and Technology*, *43*(8), 799–807. https://doi.org/10.1080/02786820902946620

Giordano, M. R., Short, D. Z., Hosseini, S., Lichtenberg, W., & Asa-Awuku, A. A. (2013). Changes in droplet surface tension affect the observed hygroscopicity of photochemically aged biomass burning aerosol. *Environmental Science & Technology*, *47*(19), 10980–10986. https://doi.org/10.1021/es401867j

Gomez, S. L., Carrico, C. M., Allen, C., Lam, J., Dabli, S., Sullivan, A. P., et al. (2018). Southwestern U.S. biomass burning smoke hygroscopicity: The role of plant phenology, chemical composition, and combustion properties. *Journal of Geophysical Research: Atmospheres*, *123*(10), 5416–5432. https://doi.org/10.1029/2017JD028162

Gramlich, Y., Siegel, K., Haslett, S. L., Cremer, R. S., Lunder, C., Kommula, S. M., et al. (2024). Impact of biomass burning on Arctic aerosol composition. *ACS Earth and Space Chemistry*, *8*(5), 920–936. https://doi.org/10.1021/acsearthspacechem.3c00187

Hall, J. (2022). Linear deming regression. MATLAB Central File Exchange. Retrieved from https://se.mathworks.com/matlabcentral/fileexchange/33484-linear-deming-regression

Han, S., Hong, J., Luo, Q., Xu, H., Tan, H., Wang, Q., et al. (2022). Hygroscopicity of organic compounds as a function of organic functionality, water solubility, molecular weight, and oxidation level. *Atmospheric Chemistry and Physics*, *22*(6), 3985–4004. https://doi.org/10.5194/acp-22-3985-2022

Haslett, S. L., Thomas, J. C., Morgan, W. T., Hadden, R., Liu, D., Allan, J. D., et al. (2018). Highly controlled, reproducible measurements of aerosol emissions from combustion of a common African biofuel source. *Atmospheric Chemistry and Physics*, *18*(1), 385–403. https://doi.org/10.5194/acp-18-385-2018

Healy, R. M., Sciare, J., Poulain, L., Crippa, M., Wiedensohler, A., Prévôt, A. S. H., et al. (2013). Quantitative determination of carbonaceous particle mixing state in Paris using single-particle mass spectrometer and aerosol mass spectrometer measurements. *Atmospheric Chemistry and Physics*, *13*(18), 9479–9496. https://doi.org/10.5194/acp-13-9479-2013

Hodshire, A. L., Akherati, A., Alvarado, M. J., Brown-Steiner, B., Jathar, S. H., Jimenez, J. L., et al. (2019). Aging effects on biomass burning aerosol mass and composition: A critical review of field and laboratory studies. *Environmental Science & Technology*, *53*(17), 10007–10022. https://doi.org/10.1021/acs.est.9b02588

Hosseini, S., Urbanski, S. P., Dixit, P., Qi, L., Burling, I. R., Yokelson, R. J., et al. (2013). Laboratory characterization of PM emissions from combustion of wildland biomass fuels. *Journal of Geophysical Research: Atmospheres*, *118*(17), 9914–9929. https://doi.org/10.1002/jgrd.50481

Hsiao, T.-C., Ye, W.-C., Wang, S.-H., Tsay, S.-C., Chen, W.-N., Lin, N.-H., et al. (2016). Investigation of the CCN activity, BC and UVBC mass concentrations of biomass burning aerosols during the 2013 BASELInE campaign. *Aerosol and Air Quality Research*, *16*(11), 2742–2756. https://doi.org/10.4209/aaqr.2015.07.0447

Jaars, K., van Zyl, P. G., Beukes, J. P., Hellén, H., Vakkari, V., Josipovic, M., et al. (2016). Measurements of biogenic volatile organic compounds at a grazed savannah grassland agricultural landscape in South Africa. *Atmospheric Chemistry and Physics*, *16*(24), 15665–15688. https://doi.org/10.5194/acp-16-15665-2016

Janhäll, S., Andreae, M. O., & Pöschl, U. (2010). Biomass burning aerosol emissions from vegetation fires: Particle number and mass emission factors and size distributions. *Atmospheric Chemistry and Physics*, *10*(3), 1427–1439. https://doi.org/10.5194/acp-10-1427-2010

Jimenez, J. L., Canagaratna, M. R., Donahue, N. M., Prevot, A. S. H., Zhang, Q., Kroll, J. H., et al. (2009). Evolution of organic aerosols in the atmosphere. *Science*, *326*(5959), 1525–1529. https://doi.org/10.1126/science.1180353

Jing, B., Peng, C., Wang, Y., Liu, Q., Tong, S., Zhang, Y., & Ge, M. (2017). Hygroscopic properties of potassium chloride and its internal mixtures with organic compounds relevant to biomass burning aerosol particles. *Scientific Reports*, *7*(1), 43572. https://doi.org/10.1038/srep43572

Kommula, S. M., Buchholz, A., Gramlich, Y., Mielonen, T., Hao, L., Pullinen, I., et al. (2024). Effect of long-range transported fire aerosols on cloud condensation nuclei concentrations and cloud properties at high latitudes. *Geophysical Research Letters*, *51*(6), e2023GL107134. https://doi.org/10.1029/2023GL107134

Köster, K., Kohli, J., Lindberg, H., & Pumpanen, J. (2024). Post-fire soil greenhouse gas fluxes in boreal Scots pine forests–Are they affected by surface fires with different severities? *Agricultural and Forest Meteorology*, *349*, 109954. https://doi.org/10.1016/j.agrformet.2024.109954

Kristensen, T. B., Falk, J., Lindgren, R., Andersen, C., Malmborg, V. B., Eriksson, A. C., et al. (2021). Properties and emission factors of cloud condensation nuclei from biomass cookstoves—Observations of a strong dependency on potassium content in the fuel. *Atmospheric Chemistry and Physics*, *21*(10), 8023–8044. https://doi.org/10.5194/acp-21-8023-2021

Kroll, J. H., Donahue, N. M., Jimenez, J. L., Kessler, S. H., Canagaratna, M. R., Wilson, K. R., et al. (2011). Carbon oxidation state as a metric for describing the chemistry of atmospheric organic aerosol. *Nature Chemistry*, *3*(2), 133–139. https://doi.org/10.1038/nchem.948

Lathem, T. L., Beyersdorf, A. J., Thornhill, K. L., Winstead, E. L., Cubison, M. J., Hecobian, A., et al. (2013). Analysis of CCN activity of Arctic aerosol and Canadian biomass burning during summer 2008. *Atmospheric Chemistry and Physics*, *13*(5), 2735–2756. https://doi.org/10.5194/acp-13-2735-2013

Leskinen, A., Yli-Pirilä, P., Kuuspalo, K., Sippula, O., Jalava, P., Hirvonen, M.-R., et al. (2015). Characterization and testing of a new environmental chamber. *Atmospheric Measurement Techniques*, *8*(6), 2267–2278. https://doi.org/10.5194/amt-8-2267-2015

Li, J., Pósfai, M., Hobbs, P. V., & Buseck, P. R. (2003). Individual aerosol particles from biomass burning in southern Africa: 2, Compositions and aging of inorganic particles. *Journal of Geophysical Research*, *108*(D13), 8484. https://doi.org/10.1029/2002JD002310

Li, Y. (2019). Cloud condensation nuclei activity and hygroscopicity of fresh and aged biomass burning particles. *Pure and Applied Geophysics*, *176*(1), 345–356. https://doi.org/10.1007/s00024-018-1903-0

Liang, Y., Stamatis, C., Fortner, E. C., Wernis, R. A., Van Rooy, P., Majluf, F., et al. (2022). Emissions of organic compounds from western US wildfires and their near-fire transformations. *Atmospheric Chemistry and Physics*, *22*(15), 9877–9893. https://doi.org/10.5194/acp-22-9877-2022

Lim, C. Y., Hagan, D. H., Coggon, M. M., Koss, A. R., Sekimoto, K., de Gouw, J., et al. (2019). Secondary organic aerosol formation from the laboratory oxidation of biomass burning emissions. *Atmospheric Chemistry and Physics*, *19*(19), 12797–12809. https://doi.org/10.5194/acp-19-12797-2019

Mao, J., Ren, X., Brune, W. H., Olson, J. R., Crawford, J. H., Fried, A., et al. (2009). Airborne measurement of OH reactivity during INTEX-B. *Atmospheric Chemistry and Physics*, *9*(1), 163–173. https://doi.org/10.5194/acp-9-163-2009

Martin, M., Tritscher, T., Jurányi, Z., Heringa, M. F., Sierau, B., Weingartner, E., et al. (2013). Hygroscopic properties of fresh and aged wood burning particles. *Journal of Aerosol Science*, *56*, 15–29. https://doi.org/10.1016/j.jaerosci.2012.08.006

McRae, D. J., Conard, S. G., Ivanova, G. A., Sukhinin, A. I., Baker, S. P., Samsonov, Y. N., et al. (2006). Variability of fire behavior, fire effects, and emissions in Scotch pine forests of Central Siberia. *Mitigation and Adaptation Strategies for Global Change*, *11*(1), 45–74. https://doi.org/10.1007/s11027-006-1008-4

Mouton, M., Malek, K. A., James, M. H., Pokhrel, R. P., Fiddler, M. N., Asa-Awuku, A. A., & Bililign, S. (2023). The hygroscopic properties of biomass burning aerosol from Eucalyptus and cow dung under different combustion conditions. *Aerosol Science and Technology*, *57*(7), 665–677. https://doi.org/10.1080/02786826.2023.2198587

Passig, J., Schade, J., Irsig, R., Kröger-Badge, T., Czech, H., Adam, T., et al. (2022). Single-particle characterization of polycyclic aromatic hydrocarbons in background air in northern Europe. *Atmospheric Chemistry and Physics*, *22*(2), 1495–1514. https://doi.org/10.5194/acp-22-1495-2022

Passig, J., Schade, J., Rosewig, E. I., Irsig, R., Kröger-Badge, T., Czech, H., et al. (2020). Resonance-enhanced detection of metals in aerosols using single-particle mass spectrometry. *Atmospheric Chemistry and Physics*, *20*(12), 7139–7152. https://doi.org/10.5194/acp-20-7139-2020

Passig, J., & Zimmermann, R. (2021). Laser ionization in single-particle mass spectrometry. In R. Zimmermann, & L. Hanley (Eds.), *Photoionization and photo-induced processes in mass spectrometry* (pp. 359–411). Wiley-VCH. https://doi.org/10.1002/9783527682201.ch11

Peltokorpi, S., Kommula, S. M., Buchholz, A., Hao, L., Ihalainen, M., Jaars, K., et al. (2025). Savannah and boreal biomass burning as a source for cloud condensation nuclei [Dataset]. *Zenodo*. https://doi.org/10.5281/zenodo.15629421

Penner, J. E., Chuang, C. C., & Grant, K. (1998). Climate forcing by carbonaceous and sulfate aerosols. *Climate Dynamics*, *14*(12), 839–851. https://doi.org/10.1007/s003820050259

Petters, M. D., Carrico, C. M., Kreidenweis, S. M., Prenni, A. J., DeMott, P. J., Collett, J. L., Jr., & Moosmüller, H. (2009). Cloud condensation nucleation activity of biomass burning aerosol. *Journal of Geophysical Research*, *114*(D22), D22205. https://doi.org/10.1029/2009JD012353

Petters, M. D., & Kreidenweis, S. M. (2007). A single parameter representation of hygroscopic growth and cloud condensation nucleus activity. *Atmospheric Chemistry and Physics*, *7*(8), 1961–1971. https://doi.org/10.5194/acp-7-1961-2007

Pokhrel, R. P., Wagner, N. L., Langridge, J. M., Lack, D. A., Jayarathne, T., Stone, E. A., et al. (2016). Parameterization of single-scattering albedo (SSA) and absorption Ångström exponent (AAE) with EC/OC for aerosol emissions from biomass burning. *Atmospheric Chemistry and Physics*, *16*(15), 9549–9561. https://doi.org/10.5194/acp-16-9549-2016

Rantanen, M., Karpechko, A. Y., Lipponen, A., Nordling, K., Hyvärinen, O., Ruosteenoja, K., et al. (2022). The Arctic has warmed nearly four times faster than the globe since 1979. *Communications Earth & Environment*, *3*(1), 1–10. https://doi.org/10.1038/s43247-022-00498-3

Reinard, M. S., & Johnston, M. V. (2008). Ion formation mechanism in laser desorption ionization of individual nanoparticles. *Journal of the American Society for Mass Spectrometry*, *19*(3), 389–399. https://doi.org/10.1016/j.jasms.2007.11.017

Riemer, N., Ault, A. P., West, M., Craig, R. L., & Curtis, J. H. (2019). Aerosol mixing state: Measurements, modeling, and impacts. *Reviews of Geophysics*, *57*(2), 187–249. https://doi.org/10.1029/2018RG000615

Rose, D., Gunthe, S. S., Mikhailov, E., Frank, G. P., Dusek, U., Andreae, M. O., & Pöschl, U. (2008). Calibration and measurement uncertainties of a continuous-flow cloud condensation nuclei counter (DMT-CCNC): CCN activation of ammonium sulfate and sodium chloride aerosol particles in theory and experiment. *Atmospheric Chemistry and Physics*, *8*(5), 1153–1179. https://doi.org/10.5194/acp-8-1153-2008

Rose, D., Nowak, A., Achtert, P., Wiedensohler, A., Hu, M., Shao, M., et al. (2010). Cloud condensation nuclei in polluted air and biomass burning smoke near the mega-city Guangzhou, China—Part 1: Size-resolved measurements and implications for the modeling of aerosol particle hygroscopicity and CCN activity. *Atmospheric Chemistry and Physics*, *10*(7), 3365–3383. https://doi.org/10.5194/acp-10-3365-2010

Royer, H. M., Pöhlker, M. L., Krüger, O., Blades, E., Sealy, P., Lata, N. N., et al. (2023). African smoke particles act as cloud condensation nuclei in the wintertime tropical North Atlantic boundary layer over Barbados. *Atmospheric Chemistry and Physics*, *23*(2), 981–998. https://doi.org/10.5194/acp-23-981-2023

Schade, J., Passig, J., Irsig, R., Ehlert, S., Sklorz, M., Adam, T., et al. (2019). Spatially shaped laser pulses for the simultaneous detection of polycyclic aromatic hydrocarbons as well as positive and negative inorganic ions in single particle mass spectrometry. *Analytical Chemistry*, *91*(15), 10282–10288. https://doi.org/10.1021/acs.analchem.9b02477

Schmidt, M., Hakkim, H., Anders, L., Kalamaš̨ikovs, A., Kröger-Badge, T., Irsig, R., et al. (2024). A solid-state IR laser for two-step desorption/ionization processes in single-particle mass spectrometry. *EGUsphere*. (preprint). https://doi.org/10.5194/egusphere-2024-2587

Schwarz, J. P., Katich, J. M., Lee, S. L., Thomson, D. S., & Watts, L. A. (2022). "Invisible bias" in the single particle soot photometer due to trigger deadtime. *Aerosol Science and Technology*, *56*(7), 623–635. https://doi.org/10.1080/02786826.2022.2064265

Sinha, P., Hobbs, P. V., Yokelson, R. J., Bertschi, I. T., Blake, D. R., Simpson, I. J., et al. (2003). Emissions of trace gases and particles from savanna fires in southern Africa. *Journal of Geophysical Research*, *108*(D13), 8487. https://doi.org/10.1029/2002JD002325

Srivastava, D., Favez, O., Petit, J.-E., Zhang, Y., Sofowote, U. M., Hopke, P. K., et al. (2019). Speciation of organic fractions does matter for aerosol source apportionment. Part 3: Combining off-line and on-line measurements. *Science of the Total Environment*, *690*, 944–955. https://doi.org/10.1016/j.scitotenv.2019.06.378

Topping, D., Barley, M., Bane, M. K., Higham, N., Aumont, B., Dingle, N., & McFiggans, G. (2016). UManSysProp v1.0: An online and open-source facility for molecular property prediction and atmospheric aerosol calculations. *Geoscientific Model Development*, *9*(2), 899–914. https://doi.org/10.5194/gmd-9-899-2016

Tyukavina, A., Potapov, P., Hansen, M. C., Pickens, A. H., Stehman, S. V., Turubanova, S., et al. (2022). Global trends of forest loss due to fire from 2001 to 2019. *Frontiers in Remote Sensing*, *3*, 825190. https://doi.org/10.3389/frsen.2022.825190

Vakkari, V., Beukes, J. P., Dal Maso, M., Aurela, M., Josipovic, M., & van Zyl, P. G. (2018). Major secondary aerosol formation in southern African open biomass burning plumes. *Nature Geoscience*, *11*(8), 580–583. https://doi.org/10.1038/s41561-018-0170-0

Vakkari, V., Kerminen, V.-M., Beukes, J. P., Tiitta, P., van Zyl, P. G., Josipovic, M., et al. (2014). Rapid changes in biomass burning aerosols by atmospheric oxidation. *Geophysical Research Letters*, *41*(7), 2644–2651. https://doi.org/10.1002/2014GL059396

Vernooij, R., Eames, T., Russell-Smith, J., Yates, C., Beatty, R., Evans, J., et al. (2023). Dynamic savanna burning emission factors based on satellite data using a machine learning approach. *Earth System Dynamics*, *14*(5), 1039–1064. https://doi.org/10.5194/esd-14-1039-2023

Wang, S., Ding, P., Lin, S., Gong, J., & Huang, X. (2021). Smoldering and flaming of disc wood particles under external radiation: Autoignition and size effect. *Frontiers in Mechanical Engineering*, *7*, 686638. https://doi.org/10.3389/fmech.2021.686638

Ward, D. E., & Radke, L. F. (1993). Emissions measurements from vegetation fires: A comparative evaluation of methods and results. In P. J. Crutzen, & J. G. Goldammer (Eds.), *Fire in the environment: The ecological, atmospheric, and climatic importance of vegetation fires* (pp. 53–77). John Wiley and Sons.

Warneke, C., Bahreini, R., Brioude, J., Brock, C. A., de Gouw, J. A., Fahey, D. W., et al. (2009). Biomass burning in Siberia and Kazakhstan as an important source for haze over the Alaskan Arctic in April 2008. *Geophysical Research Letters*, *36*(2), L02813. https://doi.org/10.1029/2008GL036194

Warneke, C., Froyd, K. D., Brioude, J., Bahreini, R., Brock, C. A., Cozic, J., et al. (2010). An important contribution to springtime Arctic aerosol from biomass burning in Russia. *Geophysical Research Letters*, *37*(1), L01801. https://doi.org/10.1029/2009GL041816

Wiedensohler, A. (1988). An approximation of the bipolar charge distribution for particles in the submicron size range. *Journal of Aerosol Science*, *19*(3), 387–389. https://doi.org/10.1016/0021-8502(88)90278-9

Wu, H., Taylor, J. W., Langridge, J. M., Yu, C., Allan, J. D., Szpek, K., et al. (2021). Rapid transformation of ambient absorbing aerosols from West African biomass burning. *Atmospheric Chemistry and Physics*, *21*(12), 9417–9440. https://doi.org/10.5194/acp-21-9417-2021

Yokelson, R., Griffith, D., & Ward, D. (1996). Open-path Fourier transform infrared studies of large-scale laboratory biomass fires. *Journal of Geophysical Research*, *101*(D15), 21067–21080. https://doi.org/10.1029/96JD01800

Yokelson, R. J., Goode, J. G., Ward, D. E., Susott, R. A., Babbitt, R. E., Wade, D. D., et al. (1999). Emissions of formaldehyde, acetic acid, methanol, and other trace gases from biomass fires in North Carolina measured by airborne Fourier transform infrared spectroscopy. *Journal of Geophysical Research*, *104*(D23), 30109–30125. https://doi.org/10.1029/1999JD900817

Zauscher, M. D., Wang, Y., Moore, M. J. K., Gaston, C. J., & Prather, K. A. (2013). Air quality impact and physicochemical aging of biomass burning aerosols during the 2007 San Diego wildfires. *Environmental Science & Technology*, *47*(14), 7633–7643. https://doi.org/10.1021/es4004137

Zhang, G., Lin, Q., Peng, L., Yang, Y., Fu, Y., Bi, X., et al. (2017). Insight into the in-cloud formation of oxalate based on in situ measurement by single particle mass spectrometry. *Atmospheric Chemistry and Physics*, *17*(22), 13891–13901. https://doi.org/10.5194/acp-17-13891-2017